Macromolecules
ARTICLE

Macromolecules **2009**, *42*, 7485–7494 **7485**
DOI: 10.1021/ma9011329

Onset of Entanglements Revisited. Dynamical Analysis

F. Lahmar,[†] C. Tzoumanekas,[‡,§] D. N. Theodorou,[‡,§] and B. Rousseau*[,†]

[†]*Laboratoire de Chimie Physique, Université Paris-Sud 11, UMR 8000 CNRS, Orsay, France,* [‡]*National Technical University of Athens, School of Chemical Engineering, Zografou Campus, GR-15780 Athens, Greece, and* [§]*Dutch Polymer Institute (DPI), P.O. Box 902, 5600 AX Eindhoven, The Netherlands*

Received May 25, 2009; Revised Manuscript Received July 22, 2009

ABSTRACT: In a series of two papers, we study the onset of entanglements and the transition from Rouse-type to reptation dynamics, in the context of dissipative particle dynamics (DPD) simulations of a coarse-grained polymer melt. A set of monodisperse systems with increasing chain length is examined. We consider both static and dynamic aspects of the problem. Part I, the preceding paper (DOI: 10.1021/ma901131c), presents a topological analysis of our systems. It deals with the continuous transition from unentangled to entangled topology, as chain length increases, at the level of primitive paths (PPs). In part II, this paper, we present the dynamics of our systems, and a comparison between topological and dynamical analysis. We utilize a coarse-grained model of polyethylene, based on the blob (or bead) picture of a polymer chain. The conservative potentials describing bead interactions are derived by a bottom-up approach. Each bead corresponds to 20 carbon atoms. Because of the large coarse-graining level, beads can easily overlap and chain contours can cross each other. We maintain chain uncrossability by introducing a segmental repulsive potential (SRP), adapted to our model. It is demonstrated that suitable parametrization of this potential can reproduce the dynamical transition from Rouse to reptation dynamics. For short chain unentangled systems, we observe a deviation from the pure Rouse behavior, attributed to the presence of chain stiffness, nonbonded interactions, and chain uncrossability, which are not considered by the Rouse model. For long chain systems, global dynamics is typical of reptation. The chain length dependence of viscosity and self-diffusion is described by power laws, with exponents equal to $+3.2$ and -2.3, respectively. A global and local (Rouse-mode) dynamical analysis, a static topological analysis, and the comparison between them, shows that topological constraints alter polymer dynamics at length scales much shorter than the length scales implied by the reptation model. This is evidenced by a slowing down of Rouse modes, which is maximum at the length scale where the underlying system of interpenetrating PPs appears as a network of topological constraints.

1. Introduction

Simulation of polymers at an atomic scale is complex because of the wide range of length and time scales of interest. Therefore, several descriptions have been developed, generally called "coarse-grained" models, all aiming at reducing both the number of particles and the computational time, while attempting to preserve at least a qualitative agreement with microscopic reality. The coarse-graining approach consists in integrating out the fast fluctuating variables of a certain number of microscopic units, which are grouped into a mesoscopic entity, henceforth called "bead". The coarse-graining level can be a few atoms, one or several monomers,[1,2] or even the whole chain.[3−5] In each case, the method used to obtain the effective bead interactions differs, ranging from iterative optimization procedures, such as the coarse-graining optimization (CG-OPT) method by Reith et al.,[6] to more straightforward methods.[2]

The dynamics of a polymer melt depends strongly on molar mass or equivalently, on molecular chain length N. When the chain length exceeds a critical value N_c, molecular motion becomes hindered by *entanglements* which tend to slow down the dynamics of the subchains whose length is greater than a characteristic length, N_e. The Rouse model,[7] and the reptation model[8,9] are the prevailing models for the dynamical description of unentangled and entangled polymers.

A systematic study of long polymer chains, at an atomistic level, by using detailed molecular dynamics simulations, while possible, for a large range of problems is computationally intractable. On the other hand, many chemical details of a polymer are unimportant for medium and large scale dynamics, as well as for investigations of basic polymer physics. Coarse grained polymer models can serve well this kind of tasks. Their use is further justified if we take into account the decrease in the number of degrees of freedom numerically treated, which gives access to much longer time and length scales.

Here, in order to conserve chemical information from the underlying atomistic model of the polymer studied, we have adopted a coarse-graining approach based on the iterative Boltzmann inversion (IBI) method.[10] In this approach, effective intermolecular and intramolecular (bonded) interaction potentials are obtained with the requirement of reproducing target correlation functions, at a given coarse-graining level.

A usual effect of the coarse-graining approach is that we have to take into account dissipative and stochastic contributions to molecular interactions. In our approach, these contributions are plugged in the DPD method, which is used for studying polymer dynamics. DPD uses soft repulsive potentials, such that chains can freely cross each other. As a consequence, a Rouse to reptation dynamical transition cannot be observed when using a standard DPD forcefield,[11] and more generally, when using soft potentials. Padding and Briels have proposed an algorithm which introduces uncrossability constraints to mesoscopic polymer melt simulations.[2] Their algorithm leads to a dynamical transition[12] with a scaling of the diffusion coefficient from $D \propto N^{-1}$ to $D \propto N^{-2}$, a transition in the scaling of the viscosity $\eta \propto N$ to $\eta \propto N^{3.6}$

*Corresponding author. E-mail: bernard.rousseau@lcp.u-psud.fr.

Published on Web 09/11/2009

above C_{400} and nonexponential relaxation behavior of the modulus. Tube diameter, entanglement molecular weight and plateau modulus are all reproduced, in good agreement with experimental data. The work presented here also considers the dynamical transition from Rouse to reptation dynamics by looking at global and local dynamic properties. However, trajectories are generated here using pairwise forces and a different algorithm, based on a segmental repulsion potential, to avoid bond crossing in DPD simulations.

In the preceding paper, from now on called part I,[13] we have presented a structural and topological analysis of the trajectories obtained from our model. In part II, this paper, we focus on the dynamical aspects of the transition from a Rouse-like to the reptation regime. We explore scaling laws for diffusion, global and local characteristic times, as well as rheological properties. We aim at comparing the dynamical results obtained through the DPD method to those obtained by topological analysis.

2. Simulation Methods and Model

2.1. Dissipative Particle Dynamics. The DPD technique was first introduced by Hoogerbrugge and Koelman[14,15] to study hydrodynamic phenomena of complex fluid systems with enhanced computational efficiency. DPD is essentially a molecular dynamics (MD) simulation where particles interact through conservative, dissipative and random forces. The equations of motion for a given particle i have the following form:

$$\dot{\mathbf{r}}_i = \mathbf{p}_i/m_i \tag{1}$$

$$\dot{\mathbf{p}}_i = \sum_{j\neq i} \mathbf{F}_{ij}^{C} + \sum_{j\neq i} \mathbf{F}_{ij}^{D} + \sum_{j\neq i} \mathbf{F}_{ij}^{R} \tag{2}$$

where $\mathbf{F}_{ij}^{C}$ is the conservative force exerted on the i-th particle by the j-th particle, $\mathbf{F}_{ij}^{D}$ is a dissipative force, and $\mathbf{F}_{ij}^{R}$ is a random force. A simple expression of the dissipative and random forces fulfilling the requirements of isotropy and Galilean invariance is:

$$\mathbf{F}_{ij}^{D} = -\gamma\omega_D(r_{ij})(\mathbf{e}_{ij}\cdot\mathbf{v}_{ij})\mathbf{e}_{ij} \tag{3}$$

$$\mathbf{F}_{ij}^{R} = \sigma\omega_R(r_{ij})\zeta_{ij}\mathbf{e}_{ij} \tag{4}$$

where $\mathbf{e}_{ij}=(\mathbf{r}_i-\mathbf{r}_j)/\|\mathbf{r}_i-\mathbf{r}_j\|$ and $\mathbf{v}_{ij}=\mathbf{v}_i-\mathbf{v}_j$ with $\mathbf{r}_i$, $\mathbf{v}_i$, the position and velocity vectors of particle i, and ζ_{ij} is a randomly fluctuating variable with Gaussian statistics: $\langle\zeta_{ij}(t)\rangle=0$ and $\langle\zeta_{ij}(t)\zeta_{i'j'}(t')\rangle = (\delta_{ii'}\delta_{jj'}+\delta_{ij'}\delta_{ji'})\delta(t-t')$. $\omega_D(r)$ and $\omega_R(r)$ are weight functions vanishing at distances larger than a certain cutoff value r_c. γ is a friction coefficient and σ controls the random force amplitude. Español and Warren showed[16] that the weight functions $\omega_D(r)$ and $\omega_R(r)$, as well as the friction coefficient γ, and the amplitude of the noise σ, could not be chosen independently. If one wants to recover the equilibrium distribution of the canonical ensemble, the following relations should be satisfied:

$$\begin{cases} [\omega_R(r)]^2 = \omega_D(r) = \omega(r) \\ \sigma^2 = 2\gamma k_B T \end{cases} \tag{5}$$

The weight function $\omega(r)$ provides the range of interaction for dissipative and random forces. In this work, following the original DPD method, this simple choice is made:

$$\omega(r) = (1-r/r_c)^2 \quad \text{for } r < r_c \tag{6}$$

$$\omega(r) = 0 \qquad \text{else} \tag{7}$$

In a preceding paper by Lahmar and Rousseau[17] we studied the influence of the adjustable parameters of the DPD on the global and local dynamics of a polymer melt. We have shown that transport coefficients can be related to the friction coefficient γ under some conditions (constant cutoff radius and coarse-graining relatively large). It is therefore possible to rescale γ so as to reproduce the experimental data. In this work, γ was chosen large enough so that dynamical processes can still be described by a dissipative particle approach, but not too large so that long-time dynamical processes can be observed. This will lead to a speed up of the dynamics compared to true material.

2.2. Coarse-Grained Model. As mentioned in the Introduction, several different procedures have been proposed to build coarse-grained models for polymer melts. Our work is based on a bottom-up approach. Interparticle interactions at the coarse level are built from interactions at the microscopic level, by using a potential of mean force approach.[18] The potentials are further refined by using the iterative Boltzmann inversion procedure.[10] Some details are given below.

The coarse-graining procedure starts with a microscopic description of the polymer melt, i.e., at an atomistic level. We have performed Monte Carlo simulations of 20 PE chains with 400 atoms per chain, at a single thermodynamic state ($T=453$ K and $P=1$ atm), using isobaric−isothermal ensemble simulations (more details in ref 18). We employ the united atom model of Karayiannis et al.[19] This force field has proven to give structural (static structure factor), conformational (charateristic ratio C_∞), and volumetric properties, in excellent agreement with available experimental data.

From the set of positions of the particles describing the polymer melt at a microscopic level, we define coarse-grained particles. We use 10 consecutive monomers (20 carbon atoms) in each chain described at the microscopic level to define a coarse-grained bead. Each bead is located at the center of mass of the corresponding particles at the atomistic level. Then, bead−bead intermolecular and intramolecular distribution functions are calculated by using coarse-grained particle positions, which are deduced from the detailed atomistic configurations, i.e., by mapping the coarse-grained model to the atomistic system. Three different distribution functions are built: the radial distribution function $g^{\mu,\mathrm{nb}}(R_{i,j})$ between coarse-grained beads belonging to different chains; the radial distribution function $g^{\mu,\mathrm{b}}(R_{i,i+1})$, between first neighbor beads in the same chain; the angular distribution function $g^{\mu,\theta}(\theta_{i-1,i,i+1})$ where θ is the angle formed by three consecutive beads in the same chain. From these distributions and using the concept of potential of mean force, we obtain potentials at the coarse-grained level:

$$w_0^{\mathrm{nb}}(R_{i,j}) = -k_B T \ln g^{\mu,\mathrm{nb}}(R_{i,j}) \tag{8}$$

$$w_0^{\mathrm{b}}(R_{i,i+1}) = -k_B T \ln g^{\mu,\mathrm{b}}(R_{i,i+1}) \tag{9}$$

$$w_0^{\theta}(\theta_{i-1,i,i+1}) = -k_B T \ln g^{\mu,\theta}(\theta_{i-1,i,i+1}) \tag{10}$$

where ${w_0}^{\mathrm{nb}}(R_{i,j})$ is the intermolecular bead−bead potential acting between beads on different chains, and between beads on the same chain separated by more than two bonds. ${w_0}^{\mathrm{b}}(R_{i,i+1})$ is the intramolecular bonding potential acting between two consecutive beads of a chain, and ${w_0}^{\theta}(\theta_{i-1,i,i+1})$ is the intramolecular bending potential.

As was shown in ref 18, when the potentials of mean force (PMF) are used in DPD simulations, the radial distribution functions for nonbonded and bonded interactions resemble the corresponding microscopic functions $g^{\mu,\mathrm{nb}}(R_{i,j})$, and $g^{\mu,\mathrm{b}}(R_{i,i+1})$. However, at this level of coarse graining, the beads in mesoscopic simulations can overlap, due to the absence of a hardcore

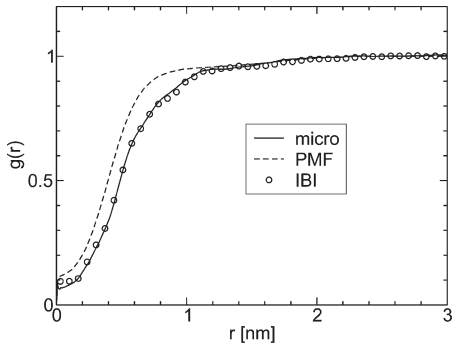

Figure 1. Pair distribution functions for nonbonded beads obtained from the mapping procedure at the microscopic level (full line), from mesoscopic simulations with the PMF (dashed line), and at the end of the iterative Boltzmann inversion procedure (open circles).

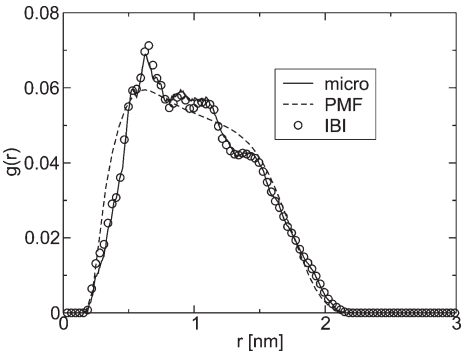

Figure 2. Pair distribution functions for bonded beads obtained from the mapping procedure at the microscopic level (full line), from mesoscopic simulations with the PMF (dashed line), and at the end of the iterative Boltzmann inversion procedure (open circles).

contribution in nonbonded interactions. Thus, excluded volume effects are underestimated, when the potentials of mean force $w_0^{nb}(R_{i,j})$ and $w_0^{b}(R_{i,i+1})$ are used in our simulations. In order to correct for this, we decided to improve the effective potentials describing nonbonded and bonded interactions by using the iterative procedure proposed by Reith et al.[10] A simulation with the potentials $w_0^{nb}(R_{i,j})$ and $w_0^{b}(R_{i,i+1})$ yields distribution functions $g_0^{nb}(R_{i,j})$ and $g_0^{b}(R_{i,i+1})$. These potentials are improved by a correction term of the form $k_BT\ln(g_0/g^{\mu})$, and the process is repeated until convergence:

$$w_{p+1}^{nb}(R_{i,j}) = w_p^{nb}(R_{i,j}) + k_BT\ln\left(\frac{g_p^{nb}(R_{i,j})}{g^{\mu,nb}(R_{i,j})}\right) \quad (11)$$

$$w_{p+1}^{b}(R_{i,i+1}) = w_p^{b}(R_{i,i+1}) + k_BT\ln\left(\frac{g_p^{b}(R_{i,i+1})}{g^{\mu,b}(R_{i,i+1})}\right) \quad (12)$$

In our case, considering a coarse-graining level of 20 carbon atoms per particle, the process converged in 4−5 iterations. The final result is a tabulated potential for bonded and nonbonded interactions, from which corresponding tabulated forces are derived.

In Figures 1 and 2, we present the results of the iterative optimization process on the radial distribution functions. A good agreement between the target distribution functions $g^{\mu,nb}(R_{i,j})$, $g^{\mu,b}(R_{i,j})$ and coarse-grained distribution functions is obtained after a few iterations. As it can be seen, the "iterated" distribution functions are in much better agreement with corresponding microscopic functions, than the crude estimates given by the potential of mean force.

2.3. Noncrossing Interactions. Because of the high coarse-graining level used here, bead−bead intermolecular interactions are much softer than Lennard-Jones interactions, and beads can easily overlap. As a consequence, unphysical bond crossing may occur: the topological constraints imposed by chain uncrossability can go away, and this may prevent the formation of entanglements. This was already pointed out by Spenley[11] in a study of polymer melts by DPD. Spenley used soft and purely repulsive conservative forces plus an harmonic potential for intramolecular bonding interactions as introduced by Hoogerbrugge and Koelman for the "classical" DPD fluid. Spenley observed that the dynamical properties of polymer melts were in very good agreement with the Rouse theory, typical of unentangled melt dynamics. However, as mentionned by Spenley: "DPD polymer chains are phantom chains who pass freely through each other" and in order to prevent bond crossing, specific interactions must be added.

Padding and Briels[2] proposed the TWENTANGLEMENT algorithm, which explicitely detects and prevents bond crossing in mesoscopic simulations of polymers. Using this algorithm they were able to reproduce entanglement effects,[12] with a scaling in the center of mass diffusion coefficient, $D_{CM} \propto N^{-2}$, and a viscosity scaling, $\eta \propto N^{3.6}$, for chains longer than 20 mesoscopic beads, (which is equivalent to 400 carbon atoms). Their approach leads to a Rouse to reptation transition for dynamical properties, but the introduction of the entanglement algorithm introduces a lot of computational overhead (the dynamics with the entanglement algorithm is roughly ten times slower than without uncrossability constraints), and the implementation of "nontrivial moves" remains tricky.

A different way to incorporate a noncrossing condition was introduced by Larson and collaborators,[20] for the study of flexible polymers in solution by Brownian dynamics, and more recently, electrophoresis of DNA in dilute polymer solutions through arrays of posts.[21] The method relies on computing the distance of closest approach between two bonds, D, and imposing a repulsive force based on that distance. In order to ensure that topological integrity is maintained (i.e., crossing events do not happen), the repulsive force must diverge as the distance of closest approach vanishes. Kumar and Larson proposed to use a repulsive potential of the form $U^{rep} \propto D^{-12}$. This is computationally expensive, however, since the steepness of the repulsive potential requires the use of very small timesteps. Indeed, they finally proposed to use an exponential function $U^{rep} \propto \exp(-\alpha D)$.

Pan and Manke[22] adopted the same approach as Kumar and Larson and used a repulsive potential of the same form as the conservative potential in DPD. This greatly reduced the frequency of chain crossing events. Moreover, with increasing chain length, the viscosity and the center of mass diffusion coefficient were shown to scale differently beyond a critical chain length. Above the critical chain length, the scaling exponent for the diffusion coefficient was found to be close to the experimental estimate of −2. These results are encouraging for the modeling of entangled polymer melt dynamics by DPD, through the use of a segmental repulsion force.

In this work, we have used the segmental repulsion model from Kumar and Larson. The form used for the segmental repulsion potential (SRP) is identical to the standard conservative potential in DPD simulations:

$$U_{rep}(D) = k_{rep}\left(1-\frac{D}{D_c}\right)^2 \quad (13)$$

where D_c is a cutoff radius beyond which the segmental repulsive potential vanishes, and k_{rep} is a force constant. The reader is referred to the paper by Kumar and Larson,[20] for the derivation and the computation of the distance of closest approach D. We notice here that the SRP algorithm increases computational time roughly by a factor of 2 compared with the same code without SRP.

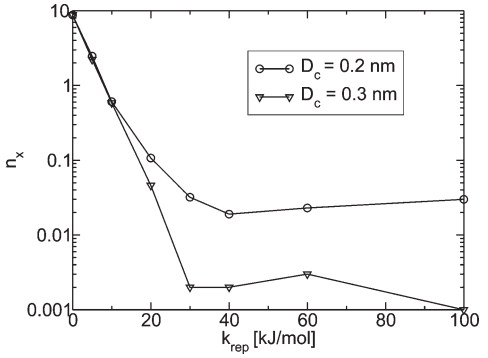

Figure 3. Average number of crossing events per step, n_x, for the whole simulation box, as a function of the force constant k_{rep}, for two different cutoff radii D_c.

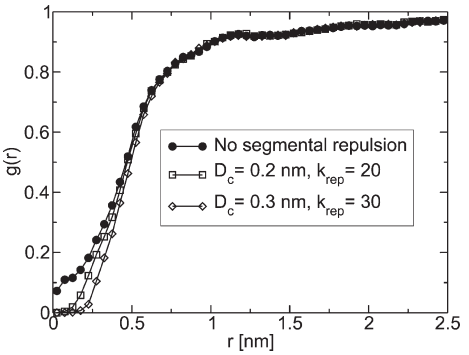

Figure 4. Effect of the segmental repulsion potential for two sets of parameters $\{D_c, k_{rep}\}$ on the pair distribution function for nonbonded interactions.

In order to evaluate the efficiency of the segmental repulsion potential with the parameters D_c and k_{rep}, we have computed the number of crossing events per step. A crossing event is recorded between bond i, defined by particle positions $\mathbf{R}_i$ and $\mathbf{R}_{i+1}$, and bond j, defined by $\mathbf{R}_j$ and $\mathbf{R}_{j+1}$, when the quantity

$$V_{ij}(t) = (\mathbf{R}_i(t) - \mathbf{R}_j(t)) \cdot [(\mathbf{R}_{i+1}(t) - \mathbf{R}_i(t)) \times (\mathbf{R}_{j+1}(t) - \mathbf{R}_j(t))] \quad (14)$$

changes sign, with an additional check to be sure that crossing is taking place along the physical part of the two finit line segments.[2] In Figure 3, we present the evolution of the average number of crossing eventsper step, for the entire system. The data were recorded during a run of 0.1 ns on a system of 80 chains with 20 beads per chain. The frequency of crossing events greatly depends on both force constant and cutoff radius. At small k_{rep} values (smaller than 20−30 kJ/mol), the number of crossing events is almost independent of D_c and decreases rapidly with k_{rep}. For large k_{rep} values, a plateau is reached for each D_c value. In this regime, the number of crossing events strongly depends on D_c. We checked that this plateau is not an artifact caused by the large value of k_{rep}. For the largest k_{rep} value, the time step was decreased by 2 orders of magnitude and the number of crossing events remained the same.

In Figure 4, we present the pair distribution function for nonbonded interactions with and without the segmental repulsion algorithm. The influence of two different sets of k_{rep} and D_c parameters is presented. Obviously, the major effect is seen at short bead−bead separations: the noncrossing algorithm creates a small excluded volume region close to the beads. This region is slightly increased when the segmental repulsion is increased, leading to an effective increase of chain thickness. This is the major drawback of the segmental repulsion method. In the Padding and Briels method, the distribution functions are not perturbed by the presence of the noncrossing algorithm. As shown in Figure 5, the introduction of the segmental repulsion has a consequence on the chain radius of gyration, R_g, which is slightly decreased. Depending on the balance between segmental repulsion intra- and intermolecular interactions, one may expect a decrease or an increase of the radius of gyration. The observed behavior indicates that, under the imposed density (constant volume), chain size decreases to relieve intermolecular segmental repulsive interactions, while the scaling $R_g^2 \propto N$ characteristic of unperturbed conformations is preserved. In this procedure the repulsion of other chains by the pervaded volume of each chain leads to the decrease of R_g.

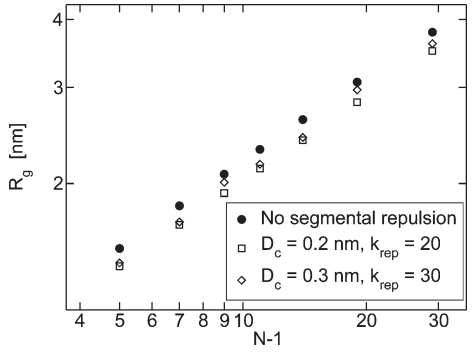

Figure 5. Effect of the segmental repulsion potential for two sets of parameters $\{D_c, k_{rep}\}$ on the radius of gyration.

3. Systems Studied

We simulated eight systems, with a number of beads per chain, N, varying from 6 to 40, as $N = 6$, 8, 10, 12, 15, 30, and 40. Each bead represents the center of mass of a $C_{20}H_{40}$ unit, and carries a corresponding mass. The DPD simulations were performed in the canonical ensemble (NVT), at a temperature of 450 K, and a density of long chain polyethylene, $\rho = 0.761$ g/cm^3, with periodic boundary conditions applied. As an integrator we have used the modified Velocity Verlet algorithm, as presented by Groot et al.[23] For the segmental repulsion potential we have used two sets of parameters: $\{D_c = 0.2$ nm, $k_{rep} = 20$ kJ/mol$\}$ and $\{D_c = 0.3$ nm, $k_{rep} = 30$ kJ/mol$\}$. In the previous section, we have seen that the first set reduces considerably the number of dynamical crossing events, but still, their number remains quite high. As will be further discussed in the document, the first set does not lead to a dynamical behavior consistent with reptation theory. Thus, except when specified, all presented results here, and in part I,[13] have been obtained with the set $\{D_c = 0.3$ nm, $k_{rep} = 30$ kJ/mol$\}$. Additional simulation details can be found in part I,[13] Table 1.

4. Results

4.1. Slowing Down of Diffusion. In this section, we investigate the mobility of the center-of-mass of the chains. For each system we computed the mean square displacement of the center-of-mass position $\mathbf{R}^{cm}$ of a chain:

$$\mathrm{msd}(t) = \langle [\mathbf{R}^{cm}(t) - \mathbf{R}^{cm}(0)]^2 \rangle \quad (15)$$

The center-of-mass self-diffusion coefficient is then given by

$$D_{CM} = \lim_{t \to \infty} \mathrm{msd}(t)/6t \quad (16)$$

We remind the reader here of the Rouse and reptation model predictions. The Rouse model treats the motion of a Gaussian chain consisting of beads in a heat bath. Interactions between beads are encompassed in a friction term ζ, and entanglements are disregarded. The Rouse prediction for the

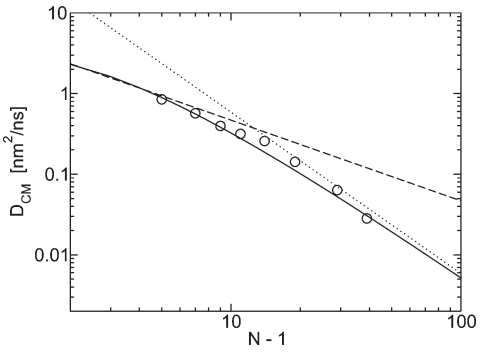

Figure 6. Center-of-mass diffusion coefficient as a function of $N - 1$. The full line corresponds to eq 17, which introduces the L_{pp} crossover. Dashed and dotted lines represent power laws with exponents of -1 and -2 respectively, and they are the corresponding asymptotes of the L_{pp} crossover presented in part I.[13]

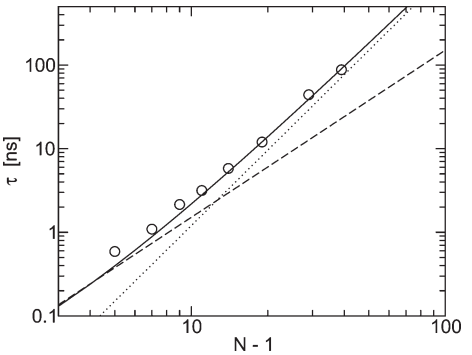

Figure 7. End-to-end decorrelation time as a function of $N - 1$. The solid line corresponds to the L_{PP} crossover prediction of eq 21. Dashed and dotted lines represent power laws with exponents of 2 and 3, respectively, and they are the corresponding asymptotes of the L_{pp} crossover presented in part I.[13]

center-of-mass self-diffusion coefficient is $D_{CM} = k_B T/\zeta N$. Experimentally, the dynamics of short polymer melts is well described by the Rouse model,[24] when the chain length dependence of ζ is taken into account.[25]

For long chain systems, the reptation model takes into account topological constraints, asserting that diffusion is hindered by entanglement interactions with surrounding chains. A test chain is forced to move inside a tube formed by entanglements with nearby chains. This kind of motion results in a slowing down of chain diffusion, and a different exponent for the scaling law: $D_{CM} \propto N^{-2}$. Lodge et al.[26] investigated the diffusion coefficient for polymer melts with chain lengths spanning the range $1 < M/M_e < 1000$. Their results suggest that $D_{CM} \propto N^{-2.3}$, with a crossover to the strict reptation power law at the highest molecular weights. The difference from the exponent predicted by the reptation model is attributed to contour length fluctuations (CLF), which take into account relaxation mechanisms that are absent in the pure reptation model, as formulated by Doi and Edwards.[9]

In Figure 6, we plot the self-diffusion coefficient as a function of chain length. Dashed lines correspond to power law exponents of -1 and -2, the predictions of Rouse and reptation models, respectively. We observe a clear change in the dynamical behavior of the melt with increasing chain length. Surprisingly, we notice a deviation from the Rouse prediction even for the shortest chains. From previous DPD simulations on a very similar system,[18] but without the segmental repulsion algorithm (i.e., chains are able to pass through each other), we know that short chains dynamics are in good agreement with Rouse theory. Consequently, even the dynamics of the shortest chains is influenced when uncrossability constraints are introduced by the segmental repulsion potential. In the next sections we will show that the effect of the SRP can also be observed in local dynamics. Also, this is consistent with the observation made in the topological analysis in part I:[13] short chains, although not properly entangled, experience topological constraints in the form of short-lived interchain contacts. A certain degree of chain interpenetration definitely exists, even for short chain systems, as evidenced by the chain overlap factor f, which is close to one (see part I[13]). This results in a slowing down of diffusion. For longer chains ($N \geq 12$), we observe a strong slowing down of diffusion, in agreement with the reptation model. More quantatively, we find that $D_{CM} \propto N^{-1.4}$ for the two shortest chain systems and $D_{CM} \propto N^{-2.3}$ for the longest chains. This last exponent is close to what is observed experimentally.

The systems simulated with $\{D_c = 0.2\ \text{nm}, k_{rep} = 20\ \text{kJ/mol}\}$ exhibit a different behavior, without showing a dynamical transition. The exponent describing the self-diffusion is equal to -1.3. Therefore, the SRP with this set of parameters does introduce uncrossability constraints into the system, but they are released too rapidly to really slow down chain diffusion.

In Figure 6, the solid line represents a prediction for the crossover of the diffusion coefficient, as estimated from the crossover of the primitive path (PP) length, L_{pp}. In the continuity of Doi's work,[27] and of what was presented in part I,[13] we have

$$D_{CM} \propto \left(\frac{L_{pp}(x)}{\sqrt{C_N(x)}} \right)^{-2} \tag{17}$$

where $x = N - 1$ is the number of bonds, and $C_N(x)$ denotes the characteristic ratio. The fit is based on just one fit parameter for shifting the curve along the y-axis. The same is true for similar fits based on L_{pp} in next sections. Since the L_{pp} crossover scheme of part I[13] suppresses CLF, it leads to a transition from Rouse to strict-reptation dynamics. As can be seen in Figure 6, the crossover regime of D_{CM} is well captured by the gradual variation of the underlying topology, which in turn is captured by the variation of the average PP length. The comparison suggests that the L_{pp} crossover indicates changes in system dynamics, and vice versa.

4.2. Reorientation of the End-to-End Vector. The end-to-end vector decorrelation time, τ, is a characteristic time of long-time systems dynamics. Reptation theory predicts that:

$$\langle \mathbf{R}_{ee}(t) \cdot \mathbf{R}_{ee}(0) \rangle = Nb^2 \psi(t) \tag{18}$$

$$\psi(t) = \sum_{k\,\text{odd}} \frac{8}{k^2 \pi^2} \exp\left(-\frac{k^2 t}{\tau} \right) \tag{19}$$

where b is the effective bond length and $\mathbf{R}_{ee}$ is the end-to-end vector. For $t \geq \tau$ we simply have

$$\langle \mathbf{R}_{ee}(t) \cdot \mathbf{R}_{ee}(0) \rangle \propto \exp\left(-\frac{t}{\tau} \right) \tag{20}$$

Reptation dynamics leads to a scaling of the form, $\tau \propto N^3$, whereas $\tau \propto N^2$, in Rouse theory. In Figure 7, we plot the end-to-end vector decorrelation time as a function of chain

length. Once again we observe a dynamical transition. The systems with chain length above $N = 12$ exhibit a behavior consistent with reptation theory. The transition occurs at approximately the same chain length as was observed for the diffusion coefficient. Again, no transition has been observed for the systems simulated with $\{D_c = 0.2$ nm, $k_{rep} = 20$ kJ/mol$\}$.

In Figure 7, the solid line represents a prediction for the crossover of the end-to-end decorrelation time as estimated from the L_{pp} crossover (see part I[13]). We have indeed:

$$\tau \propto x\left(\frac{L_{pp}(x)}{\sqrt{C_N(x)}}\right)^2 \tag{21}$$

Again, there is very good agreement in the location of the diffuse crossover regime, from static PP calculations and dynamical properties. As far as the global dynamics is concerned, the set $\{D_c = 0.3$ nm, $k_{rep} = 30$ kJ/mol$\}$ leads to a clear transition between two regimes: for the shortest chains we see a regime that differs from both the Rouse and reptation theory. For the longest chains, we see a regime consistent with reptation theory. In a previous work,[18] concerning phantom chain simulations of the same model (without a SRP), global chain dynamics were found to be in agreement with Rouse theory. Therefore, the introduction of the SRP alters global dynamics at all length scales.

4.3. Local Dynamics. We will now focus on local dynamics of polymer chains. In the framework of the Rouse model, bead motions are represented by Langevin equations whose solutions can be found by using the "Rouse modes". These modes are defined as

$$\mathbf{X}_k(t) = \frac{1}{N}\sum_{i=1}^{N}\mathbf{R}_i(t)\cos\left(\frac{k\pi}{N}\left(i-\frac{1}{2}\right)\right)$$
$$k = 1, ..., N-1 \tag{22}$$

where $\mathbf{X}_k$ represents the local motion of a subchain including N/k segments. The normalized self-correlation functions of these modes are given as

$$C_k(t) = \langle \mathbf{X}_k(t)\cdot\mathbf{X}_k(0)\rangle/\langle \mathbf{X}_k(0)^2\rangle = \exp\left(-\frac{t}{\tau_k}\right) \tag{23}$$

with $\tau_k = \zeta b^2/[12k_BT\sin^2(k\pi/2N)]$.

By a Rouse mode analysis we can shed some light to the relaxation of polymer chains at various length scales. The analysis corresponds to the reduction of the dynamics of an ideal Gaussian chain to independent normal modes, which decay exponentially, with length scale dependent relaxation times, τ_k. The Rouse modes were examined for the two sets of SRP parameters presented previously, as well as for the case where segmental repulsion was excluded from our simulations. The latter case corresponds to a reference model,[18] which is by construction free of topological constraints (phantom chain simulations).

For the Rouse mode autocorrelations, it has been established[28,29] that a more successful description is given by a stretched exponential form:

$$C_k(t) = \exp[-(t/\tau_k^*)^{\beta_k}] \tag{24}$$

where the relaxation times τ_k* and the stretching parameters β_k depend on mode number k and on chain length. The stretching parameters signify a deviation from Rouse theory.

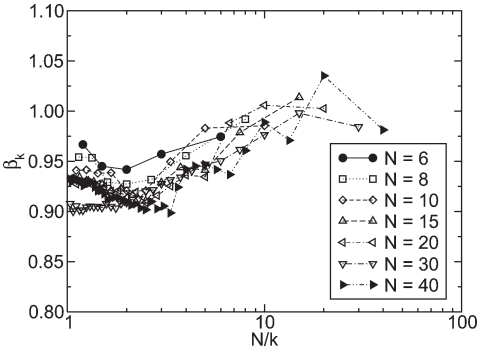

Figure 8. Stretching parameters as a function of the wavelength N/k without segmental repulsion.

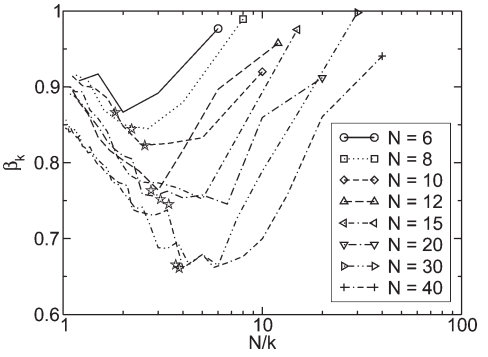

Figure 9. Stretching parameters as a function of the wavelength N/k. The stars denote N_{TC}* values from Table 3 in part I.[13]

Corresponding effective relaxation times, τ_k, for a stretched exponential form, are given by the Euler function:

$$\tau_k = \frac{\tau_k^*}{\beta_k}\Gamma\left(\frac{1}{\beta_k}\right) \tag{25}$$

such that $\tau_k = \tau_k$*, when $\beta_k = 1$, (exponential relaxation).

In Figure 8 and Figure 9, we plot the parameters β_k as a function of N/k, for all systems, as simulated in the absence and presence of segmental repulsion, respectively. In the former case, we first notice that the β_k parameters are smaller than 1.0, indicating a deviation from Rouse dynamics, but greater than 0.9, for all systems. This slight deviation may be due to chain stiffness and nonbonded interactions, which are not present in the Rouse model.

For the systems simulated with segmental repulsion, presented in Figure 9, we observe that β_k are also smaller than 1.0 for all systems. At the smallest length scales, β_k is approximately 0.9 for the shortest chain lengths, and 0.85 for $N = 30$ and $N = 40$. We also observe a minimum for each curve, but this minimum seems to depend on N. The longer the chains are, the more this minimum is shifted toward larger wavelengths. In addition, β_k increases with the wavelength, for all systems, and tends to a value larger than 0.9. Padding et al.[12] made the same investigation on a similar model. Although their stretching parameters are quite different, they also observe a minimum in β_k, but they see no dependence on N. The minimum was associated with a slowing down length scale in dynamics, denoted by N_s in ref 12, due to the presence of uncrossability constraints.

The nonexponential relaxation of the Rouse modes is not specific to our model, or to a mesoscopic approach. It is a result of the fact that the Rouse modes are not the normal modes of the simulated dynamics. Shaffer[28] investigated the behavior of β_k for uncrossable and phantom chains, by using

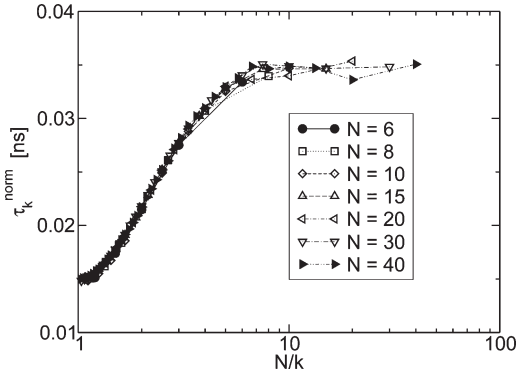

Figure 10. Normalized effective relaxation times as a function of the wavelength N/k for different chain lengths without segmental repulsion.

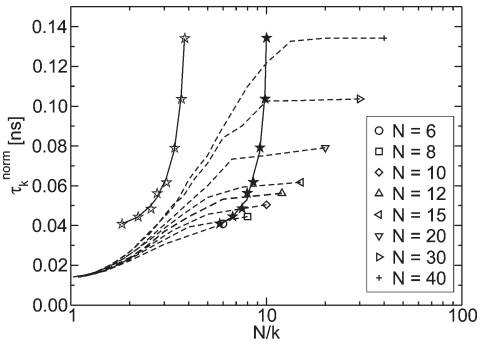

Figure 11. Normalized effective relaxation times as a function of the wavelength N/k for different chain lengths. Open stars denote N_{TC}* values (see Table 3 from paper part I[13]) plotted at an ordinate equal to the maximum of each curve. Filled stars denote N_e values plotted in the same way.

on-lattice simulations. The presence of nonexponential relaxation was interpreted in the context of the dynamical model of hierarchical constraints.[30] In the framework of this model, the existence of a stretched exponential in the relaxation of the k mode indicates the presence of a hierarchy of kinetic constraints, which leads to dynamical correlations between different modes, and involves a certain degree of cooperativity between these modes during relaxation. The deviation of β_k from unity can then be regarded as an indicator of the severity of kinetic constraints for the corresponding length scale.

The presence of nonexponential relaxations can also be interpreted in the framework of cooperative dynamics and the mode coupling model, developed by Ngai et al.[31,32] This model defines a time t_c characterizing the transition from short-time Rouse dynamics to entangled dynamics. For times $t > t_c$, the relaxation of modes is slowed down by entanglements, and the relaxation rates τ_k show a dependence $(t/t_c)^{-n_k}$, where n_k is an input, 'coupling parameter' of the model, such that $0 < n_k < 1$. It can be shown that the decorrelation function of mode k is a stretched exponential, with a stretching parameter given by $\beta_k = 1 - n_k$.

These two models help us to give an interpretation to the stretching parameters β_k, which is rather qualitative. A quantitative indication from Figure 9 is that kinetic constraints due to uncrossability are more severe between $N/k = 2$ and $N/k = 4$, depending on chain length. In this figure we also plot by stars the N_{TC}* values, deduced by the topological analysis in part I.[13] N_{TC}* is the average length between successive topological constraints along *constrained* chains. It is the average length scale where primitive paths experience the effect of chain uncrossability. Moreover, collectively, the PPs of *constrained chains* generate an underlying network with an average mesh length equal to N_{TC}*. For each curve, N_{TC}* is plotted at an ordinate equal to the minimum value of β_k. We see that the length scale defined by TCs correlates well with the minimum in β_k determined by Rouse mode analysis. We also note that N_{TC}* denotes an average value, and in general it follows a distribution[33−35] with an exponential tail. Therefore, TCs influence dynamics at several length scales around N_{TC}*.

The effect of TCs can also be traced by plotting the normalized relaxation times, τ_k^{norm},

$$\tau_k^{norm} = \tau_k \times \sin^2(k\pi/2N) \tag{26}$$

as a function of wavelength N/k. In Rouse theory, τ_k^{norm} are chain length (N) and length scale (k) independent. Thus, in a plot of τ_k^{norm} versus N/k, the curves for various N would all collapse to a horizontal straight line. In Figure 10 and Figure 11, we present τ_k^{norm} for systems simulated without (phantom chains) and with segmental repulsion, respectively. For the systems simulated in the absence of a SRP, we see that though chain length independence is present, there is a deviation from the Rouse prediction: the modes are slowed down homogeneously for short wavelengths. As in Figure 8, this must be due to the existence of short-lived constraints originating from nonbonded interactions, and chain stiffness. For the systems simulated with segmental repulsion, the deviation from the Rouse prediction is much clearer. For small wavelengths the data collapse on the same curve. This regime is below the length scale defined by N_{TC}*. The latter is plotted in Figure 11 by open stars, at an ordinate equal to the maximum of each curve. As the wavelength increases, the relaxation times grow rapidly with N/k, and the data for the longest chains reach a plateau at a value that differs for each chain length. The relaxation times for the first few modes of the long chains are consistent with the predictions of reptation theory. Indeed, the values of the different plateau for the longest chains are proportional to N, which is consistent with the prediction $\tau_k \propto N^3/k^2$. For intermediate wavelengths, the dependence of normalized relaxation times is different from both the Rouse and reptation predictions.

The effect of entanglements seems to apply totally to the dynamics of long chains for $N/k \geq 10$. This suggests that N_e is of the order, or smaller, than 10. This is in very good agreement with the topological analysis estimation $N_e(N) \simeq 10$, from the long chain systems ($N = 30,40$). Topological estimations of N_e for all chain lengths are plotted in Figure 11 with filled stars, at an ordinate equal to the maximum of each curve. We observe a good correlation of N_e with the length scale where curves bend and start to generate a plateau, consistent with reptation theory.

The local dynamics of polymer chains lets new characteristic length scale regimes to appear: the first one is related to a minimum in the stretching parameters β_k. The second one characterizes a transition of the local dynamics into a regime that is distinct from both the Rouse and the reptation theory and correlates very well with the length scales between N_{TC}* and N_e determined by topological analysis. The third regime is signified by a plateau in the normalized times, which is consistent with reptation theory.

We have made the same analysis for systems simulated with the set of parameters $\{D_c = 0.2\,\text{nm}, k_{rep} = 20\,\text{kJ/mol}\}$, for the SRP. The results for τ_k^{norm} are shown in Figure 12. They are similar to those of Figure 11. Three regimes are observed, but the general dependence does not show a distinct, linear on N "plateau", indicating that the full reptation regime is not attained. The slowing down of dynamics remains selective,

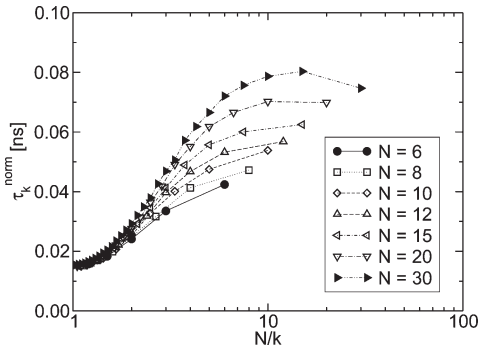

Figure 12. Normalized effective relaxation times as a function of the wavelength N/k for different chain lengths with $D_c = 0.2$ nm and $k_{rep} = 20$ kJ/mol.

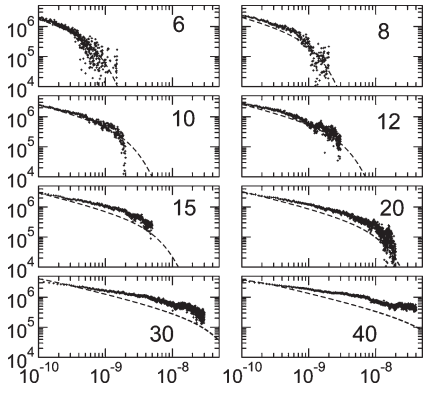

Figure 13. Shear relaxation modulus in Pa, versus time in seconds, for different chain lengths as obtained from DPD simulations. Dashed lines are Rouse predictions, obtained by using measured end-to-end vector decorrelation times as inputs.

as far as the modes are concerned, but this slowing down is weaker than what is obtained with the other set of SRP parameters.

4.4. Rheological Properties. In this section, we investigate rheological properties of our systems. The shear relaxation modulus of polymer melts exhibits a characteristic plateau, due to entanglements, that simulation works have tried to reproduce.[12] The relaxation of these liquids is believed to follow two different regimes. The initial relaxation follows the Rouse model:

$$G(t) = \frac{ck_BT}{N}\sum_{k=1}^{N-1}\exp(-2t/\tau_k) \tag{27}$$

where c is the number concentration of blobs. The crossover time between the Rouse and the reptation regime, defining the plateau, is the entanglement time, τ_e.

Reptation theory predicts a time dependence of the long-time shear relaxation as follows:

$$G(t) = G_N^0\psi(t) \tag{28}$$

where $\psi(t)$ was introduced previously, and G_N^0 is the plateau modulus. In this framework, the $\psi(t)$ function is directly linked to the end-to-end vector decorrelation time.

We computed shear relaxation moduli from the autocorrelation of the stress tensor elements. For each system, we computed the corresponding Rouse model prediction by using the measured end-to-end vector relaxation time as input for $G(t)$. The zero-shear viscosity can then be computed by integration of the shear relaxation modulus.

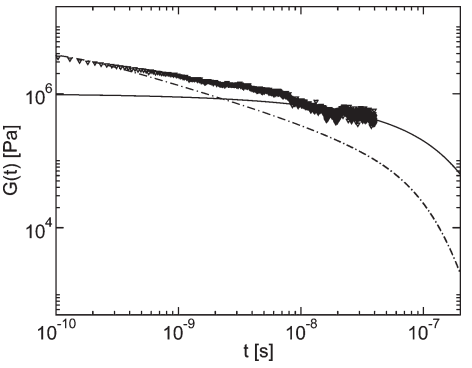

Figure 14. Shear relaxation modulus for $N = 40$. The full line represents the scaled ψ function. The dotted line represents the Rouse prediction.

In Figure 13, we plot the shear relaxation moduli and the corresponding Rouse predictions (eq 27, with τ_1 value corresponding to the end-to-end vector relaxation time and $\tau_k = \tau_1/k^2$). Theoretically, the entanglement mass could be determined either from an estimation of τ_e, or from the plateau modulus via the formula:

$$G_N^0 = \frac{4}{5}\frac{\rho RT}{M_e} \tag{29}$$

The M_e value should be taken with care. In general, a difference is observed between the entanglement masses, as determined from the plateau modulus or from the dynamics. The relation between the plateau modulus and the entanglements mass has been obtained through an analogy between entangled and idealized cross-linked systems. Consequently, eq 29 is quite empirical and M_e values obtained by the two above mentionned approaches usually do not match.[36]

The distribution of normalized relaxation times has shown that there is not a clear-cut separation between modes which are affected by the presence of entanglements, and modes that are not affected. We rather observe an intermediate behavior. Therefore, we expect that the transition in the shear relaxation modulus, between the unentangled and the entangled regime, will be somewhat smoother than predicted by theory, which will make the determination of τ_e difficult. Indeed, in Figure 13, the shear relaxation moduli exhibit no obvious characteristic time linked to a change of shape which could be associated with τ_e. However, above $N = 12$, the Rouse predictions clearly differ from simulated data. This leads to an estimation of N_e around 10.

For $N = 30$ and $N = 40$, we computed the $\psi(t)$ function and adjusted the proportionality factor to fit it with our data. This factor should be equal to the plateau modulus. Using this method, we find that $N_e \approx 8$. This value should be taken with care since we use a model to determine it. Moreover this factor is determined from the long-time behavior of $G(t)$ for which we have quite poor statistics. In Figure 14, we plot the computed shear relaxation modulus for $N = 40$, the Rouse prediction and the scaled ψ function used to fit $G(t)$.

Inversely, we can use the N_e values obtained by topological analysis in part I,[13] and the end-to-end vector decorrelation times obtained here, in order to compute predictions for the shear relaxation modulus. We used two models, the original Doi–Edwards model[9] and the Milner–McLeish model.[37] These models are compared to our data in Figure 15 and Figure 16 for $N = 30$ and $N = 40$, respectively. A good agreement between simulated data and models is again attained, especially with the Milner–McLeish model. This indicates the good consistency between topological data and dynamical data (within the predictive capability of the models).

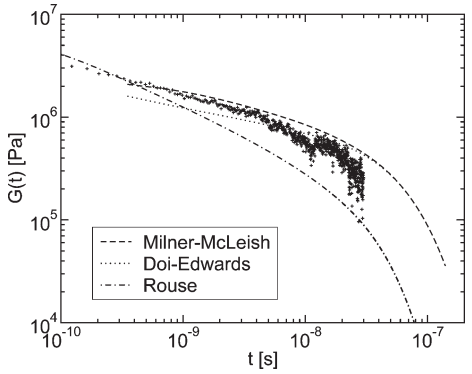

Figure 15. Computed shear relaxation modulus for $N = 30$. Comparison with different models using N_e as determined by topological analysis and end-to-end vector decorrelation time obtained from DPD simulations.

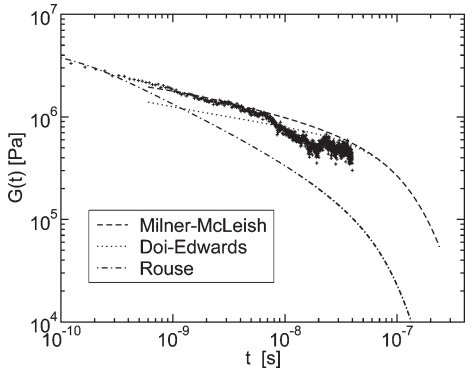

Figure 16. Same legend as in Figure 15, for a chain length $N = 40$.

Finally, the zero-shear viscosity is plotted in Figure 17. Experimentally, if one measures the viscosity for different molecular weights, a transition between two regimes is observed. Theoretically these regimes are again identified as the Rouse and reptation regimes.[9] Nevertheless, the exponents found experimentally are different from those predicted by theory. Pearson et al.[38] found that the chain length viscosity dependence could be represented by a power law

$$\eta \propto N^{\alpha} \tag{30}$$

with $\alpha = 1.8$ at low molecular weight, and $\alpha = 3.6$ at high molecular weight. The transition occurs at a mass that is characteristic of each polymer, the critical mass M_c.

Our data are plotted in Figure 17. We see clearly two regimes. For the shortest chains, the viscosity can be represented by a power law with an exponent equal to 1.5. For the longest chains, this exponent is equal to 3.2. The transition occurs between $N = 8$ and $N = 15$, corresponding to a critical mass, M_c between 2240 and 4200 $g \cdot mol^{-1}$. As the viscosity is the integral of the shear modulus, we can try to understand the role of the critical mass by looking at Figure 13. Concerning viscosity, for systems with mass below the critical mass, we do not expect to find the exact exponent of the Rouse model, when $G(t)$ cannot be fitted by the Rouse model prediction. For these systems, we have seen that topological constraints already play a role and slow down the dynamics. On the other hand, for systems with a mass above the critical mass, the shear modulus clearly deviates from the Rouse prediction. For these systems, we also observe a plateau in the plot of normalized relaxation, for long wavelengths. In Figure 17, we also plot

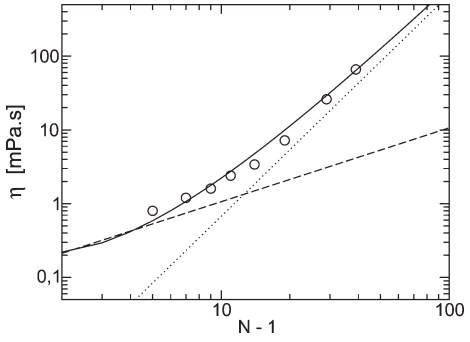

Figure 17. Zero-shear viscosity as a function of $N - 1$. The solid line corresponds to the L_{PP} crossover prediction of eq 31. Dashed and dotted lines represent power laws with exponents of 1 and 3 respectively, and they are the corresponding asymptotes of the L_{pp} crossover presented in part I.[13]

the prediction for viscosity based on L_{pp} calculations and in the scaling formula

$$\eta \propto \frac{1}{x}\left(\frac{L_{pp}(x)}{\sqrt{C_N(x)}}\right)^4 \tag{31}$$

presented in part I.[13] This prediction is based on a model which suppresses CLF, which play a crucial role in dynamics at moderate chain lengths. The agreement in the location of the crossover by static and dynamic calculations is good, but not quantitative. The L_{pp} crossover leads to an M_c/M_e ratio equal to 1. The reader is directed to part I[13] for a discussion on this issue.

5. Conclusions

In a series of two papers, parts I[13] and II, we have presented a multiscale analysis of the onset of entanglements in a coarse-grained polymer melt. We utilized a model that is based on a bottom-up approach, and the blob picture of a polymer chain. Starting from a microscopic description of a polyethylene melt, at an atomistic level, a coarse-graining procedure reduced the number of degrees of freedom which were then considered in melt dynamics. The procedure replaces a specific number of consecutive chain monomers with a single bead (blob).

At the coarse-grained level, conservative potentials were obtained using a potential of mean force approach, followed by a refinement based on an iterative Boltzmann inversion (IBI) procedure. The coarse-grained potentials permit chain crossing, thus, a further term was added to the set of interactions to prevent bond crossing: the segmental repulsion potential (SRP). The dynamics of short and long chain model systems were then generated by the DPD method. We have shown that segmental repulsion, although it slightly modifies structural properties, leads to an N-dependence of dynamical properties, like self-diffusion and viscosity, in agreement with the universal picture of polymer melt dynamics.

The DPD trajectories were further coarse-grained at the level of shortest paths, which we consider as realizations of the primitive paths (PPs).[9] Collectively, the shortest paths are interconnected to form a network, where the vertices are considered as topological constraints (TCs), or slip links, restricting a pair of chains.[33] The length scales characterizing shortest paths are, N_{TC}*, the average mesh length of the network part of the system, and N_e, the average length scale where PPs can be viewed as random walks (RWs). From our multiscale, static, and dynamic analysis in parts I[13] and II, the following picture of the onset of entanglements can be given.

In short chain systems the PPs resemble rod-like objects, and there is a small concentration of TCs. A part of the system is network-like (since some chains are unconstrained), and TCs act as short-lived interchain contacts. Actually, it is our static approach, based on shortest paths, which in this regime reveals interchain contacts in a form of a network. Moreover, system dynamics show that the short TC lifetimes are not sufficient to produce reptation-like dynamics. However, as chain length increases, PPs become progressively zigzag shaped lines, the network mesh increases asymptotically, and the longer TC lifetimes lead to reptation.

In the time domain the constraints influence local dynamics, as evidenced by the behavior of the stretching parameter β_k. This parameter can be regarded as an indicator of the severity of the kinetic constraints at a given length scale, typically N/k. We have found that the largest deviation of β_k from Rouse behavior occurs at a length scale which can be identified with the network mesh, N_{TC}*. This length scale also appears in the evolution of the normalized effective relaxation times, τ_k^{norm}. For Rouse modes corresponding to a length scale larger than N_{TC}*, τ_k^{norm} departs from a pure Rouse behavior. Therefore, the TCs determined by static topological analysis appear in the dynamics as kinetic constraints slowing down Rouse modes, and *vice versa*.

Dynamically, the onset of entanglements is a gradual transition, as observed in the chain length dependence of the diffusion coefficient and the zero shear rate viscosity. From the static point of view, and at the level of PPs, we have seen that, as chain length increases, there is also a continuous gradual transformation of PP conformations from thin rod-like objects, to random walks. This transformation leads to a crossover in the chain length dependence of the average PP length. In the rod regime, $L_{pp} \propto C_N^{1/2} N^{1/2}$, while in long chain systems, $L_{pp} \propto N$. On the basis of earlier work of Doi,[27] this "static" L_{pp} crossover was associated and compared with the onset of entanglements in the time domain. We have found that the location of the crossover regime in dynamical properties is in qualitative agreement with the predictions of static L_{pp} calculations. Inclusion of contour length fluctuations in the L_{pp} crossover scheme is a promising improvement for a future quantitative comparison.

Acknowledgment. J.-M. Teuler is acknowledged for optimization and parallelization of the DPD code. The IDRIS supercomputing center (Orsay, France) is gratefully acknowledged for a generous allocation of computer time. The work of C.T. and D.N.T., in the context of this paper, is part of the Research Programme of the Dutch Polymer Institute (DPI), Eindhoven, The Netherlands, project No. 650.

References and Notes

(1) Akkermans, R. L. C.; Briels, W. J. *J. Chem. Phys.* **2000**, *113*, 6409–6422.
(2) Padding, J. T.; Briels, W. J. *J. Chem. Phys.* **2001**, *115*, 2846–2859.
(3) Murat, M.; Kremer, K. *J. Chem. Phys.* **1998**, *108*, 4340–4348.
(4) Louis, A. A.; Bolhuis, P. G.; Hansen, J. P.; Meijer, E. *J. Phys. Rev. Lett.* **2000**, *85*, 2522–2525.
(5) Bolhuis, P. G.; Louis, A. A.; Hansen, J. P. *J. Chem. Phys.* **2001**, *114*, 4296–4311.
(6) Reith, D.; Meyer, H.; Müller-Plathe, F. *Comput. Phys. Commun.* **2002**, *148*, 299–313.
(7) Rouse, P. E. *J. Chem. Phys.* **1953**, *21*, 1272–1280.
(8) de Gennes, P. G. *Scaling concepts in polymer physics*; Cornell University Press: Ithaca, NY, 1979.
(9) Doi, M.; Edwards, S. F. *The theory of polymer dynamics*; Clarendon Press: Oxford, U.K., 1986.
(10) Reith, D.; Pütz, M.; Müller-Plathe, F. *J. Comput. Chem.* **2003**, *14*, 1624–1636.
(11) Spenley, N. A. *Europhys. Lett.* **2000**, *49*, 534–540.
(12) Padding, J. T.; Briels, W. J. *J. Chem. Phys.* **2002**, *117*, 925–943.
(13) Tzoumanekas, C.; Lahmar, F.; Rousseau, B.; Theodorou, D. N. *Macromolecules* **2009**, 10.1021/ma901131c.
(14) Hoogerbrugge, P. J.; Koelman, J. M. V. A. *Europhys. Lett.* **1992**, *19*, 155–160.
(15) Koelman, J. M. V. A.; Hoogerbrugge, P. J. *Europhys. Lett.* **1993**, *21*, 363–368.
(16) Español, P. *Phys. Rev. E* **1995**, *52*, 1734–1742.
(17) Lahmar, F.; Rousseau, B. *Polymer* **2007**, *48*, 3584–3592.
(18) Guerrault, X.; Rousseau, B.; Farago, J. *J. Chem. Phys.* **2004**, *121*, 6538–6546.
(19) Karayiannis, N. C.; Giannousaki, A. E.; Mavrantzas, V. G.; Theodorou, D. N. *J. Chem. Phys.* **2002**, *117*, 5465–5479.
(20) Kumar, S.; Larson, R. G. *J. Chem. Phys.* **2001**, *114*, 6937–6941.
(21) Holleran, S. P.; Larson, R. G. *Rheol. Acta* **2008**, *47*, 3–17.
(22) Pan, G.; Manke, C. *Int. J. Mod. Phys. B* **2003**, *17*, 231–235.
(23) Groot, R. D.; Warren, P. B. *J. Chem. Phys.* **1997**, *107*, 4423–4435.
(24) Paul, W.; Smith, G. D. *Rep. Prog. Phys.* **2004**, *67*, 1117–1185.
(25) Pearson, D. S.; Fetters, L. J.; Graessley, W. W.; ver Strate, G.; von Meerwall, E. *Macromolecules* **1994**, *27*, 711–719.
(26) Lodge, T. P. *Phys. Rev. Lett.* **1999**, *83*, 3218–3221.
(27) Doi, M. *J. Phys. A: Math. Gen.* **1975**, *8*, 417–426.
(28) Shaffer, J. S. *J. Chem. Phys.* **1995**, *103*, 761–772.
(29) Paul, W.; Smith, G. D.; Yoon, D. Y. *Macromolecules* **1997**, *30*, 7772–7780.
(30) Palmer, R. G.; Stein, D. L.; Abrahams, E.; Anderson, P. W. *Phys. Rev. Lett.* **1984**, *53*, 958–961.
(31) Ngai, K.; Skolnick, J. *Macromolecules* **1991**, *24*, 1561–1566.
(32) Ngai, K.; Peng, S.; Skolnick, J. *Macromolecules* **1992**, *25*, 2184.
(33) Tzoumanekas, C.; Theodorou, D. N. *Macromolecules* **2006**, *39*, 4592–4604.
(34) Spyriouni, T.; Tzoumanekas, C.; Theodorou, D. N.; Müller-Plathe, F.; Milano, G. *Macromolecules* **2007**, *40*, 3876–3885.
(35) Foteinopoulou, K.; Karayiannis, N. C.; Laso, M.; Kröger, M.; Mansfield, M. L. *Phys. Rev. Lett.* **2008**, *101*, 265702.
(36) Padding, J.; Briels, W. *J. Chem. Phys.* **2004**, *120*, 2996–3002.
(37) Milner, S.; McLeish, T. *Phys. Rev. Lett.* **1998**, *81*, 725.
(38) Pearson, D. S.; ver Strate, G.; von Meerwall, E.; Schilling, F. C. *Macromolecules* **1987**, *20*, 1133–1141.